BMC Neuroscience

RESEARCH

Open Access

Dorsal root ganglion inflammation by oxaliplatin toxicity: DPEP1 as possible target for peripheral neuropathy prevention

Karen Álvarez-Tosco[1,2,3†], Rebeca González-Fernández[1,8†], María Ángeles González-Nicolás[4,10], Rita Martín-Ramírez[1,8], Manuel Morales[5], Ricardo Gutiérrez[6], Lucio Díaz-Flores[6], María Rosa Arnau[7], Félix Machín[2,8,9], Julio Ávila[1,8], Alberto Lázaro[4,10*†] and Pablo Martín-Vasallo[1,8*†]

Abstract

Background Peripheral neuropathy (PN) constitutes a dose-limiting side effect of oxaliplatin chemotherapy that often compromises the efficacy of antineoplastic treatments. Sensory neurons damage in dorsal root ganglia (DRG) are the cellular substrate of PN complex molecular origin. Dehydropeptidase-1 (DPEP1) inhibitors have shown to avoid platin-induced nephrotoxicity without compromising its anticancer efficiency. The objective of this study was to describe DPEP1 expression in rat DRG in health and in early stages of oxaliplatin toxicity. To this end, we produced and characterized anti-DPEP1 polyclonal antibodies and used them to define the expression, and cellular and subcellular localization of DPEP1 by immunohistochemical confocal microscopy studies in healthy controls and short term (six days) oxaliplatin treated rats.

Results DPEP1 is expressed mostly in neurons and in glia, and to a lesser extent in endothelial cells. Rats undergoing oxaliplatin treatment developed allodynia. TNF-α expression in DRG revealed a pattern of focal and at different intensity levels of neural cell inflammatory damage, accompanied by slight variations in DPEP1 expression in endothelial cells and in nuclei of neurons.

Conclusions DPEP1 is expressed in neurons, glia and endothelial cells of DRG. Oxaliplatin caused allodynia in rats and increased TNF-α expression in DRG neurons. The expression of DPEP1 in neurons and other cells of DRG suggest this protein as a novel strategic molecular target in the prevention of oxaliplatin-induced acute neurotoxicity.

Keywords Dorsal root ganglion (DRG), Oxaliplatin, Neurotoxicity, DRG-inflammation, Dehydropeptidase-1 (DPEP1), Allodynia

†Karen Álvarez-Tosco and Rebeca González-Fernández contributed equally to this article. Both are first author.

†Alberto Lázaro and Pablo Martín-Vasallo contributed equally to this work and share senior authorship

*Correspondence:
Alberto Lázaro
alberlaz@ucm.es
Pablo Martín-Vasallo
pmartin@ull.edu.es

Full list of author information is available at the end of the article

© The Author(s) 2024. **Open Access** This article is licensed under a Creative Commons Attribution-NonCommercial-NoDerivatives 4.0 International License, which permits any non-commercial use, sharing, distribution and reproduction in any medium or format, as long as you give appropriate credit to the original author(s) and the source, provide a link to the Creative Commons licence, and indicate if you modified the licensed material. You do not have permission under this licence to share adapted material derived from this article or parts of it. The images or other third party material in this article are included in the article's Creative Commons licence, unless indicated otherwise in a credit line to the material. If material is not included in the article's Creative Commons licence and your intended use is not permitted by statutory regulation or exceeds the permitted use, you will need to obtain permission directly from the copyright holder. To view a copy of this licence, visit http://creativecommons.org/licenses/by-nc-nd/4.0/.

Background

Platinum-based chemotherapy agents have been widely used against a variety of solid tumors since its discovery in the 1970s. However, these compounds have several serious side effects that limit their efficacy [1, 2]. Neurotoxicity, more frequently associated with cisplatin and oxaliplatin (OxPt), which cannot be prevented or tackled, constitutes a serious dose-limiting side effect, and modifies the expression level of a large number of genes [3]. The majority of patients treated with OxPt (80–90%) experience any grade of neurotoxicity [4–6] requiring dose adjustments or discontinuation, which could compromise treatment efficacy and clinical objectives achievement [7].

OxPt-induced peripheral neuropathy (PN) is a clinically separate syndrome characterized by multiple symptoms as a result of sensory neuronal cell damage and death. The intensity of symptoms varies from very low to high degree of disability. Positive sensory symptoms and loss of function signs appear in upper and lower limbs, such as: numbness, tingling, paresthesia and neuropathic pain, reduction touch sensation, vibration and absence of tendon reflexes [8]. Acute peripheral neurotoxicity of OxPt has been described with transient paresthesia, dysesthesia and muscle cramps induced by cold exposure (cold allodynia). This phenomenon is associated with the development of chronic PN, which occurs with increasing cumulative dosage [7–10]. These facts can be imitated in experimental animal models [11, 12]. Pathogenesis of this syndrome is unclear; however, it is focused on platinum toxicity over primary sensory neurons at the dorsal root ganglia (DRG) [7]. Furthermore, OxPt impairs nodal axonal voltage-gated Na+channels and, oxalate released after its metabolism may be related to acute cold-induced hypersensitivity [13, 14]. Relieving of pain elicited by chemotherapy side effects has been assessed in rodent models by targeting several receptors as Mu-Opioid receptor agonist [15, 16] and TRP channels [12, 17, 18].

The damage elicited by OxPt in neurons of DRG, as well as other kind of cells has been associated with excessive production of reactive oxygen species due to decreased antioxidant enzymes [19, 20]. Dehydropeptidase-1 (DPEP1) hydrolyses different dipeptides, including glutathione (GSH), which is a key molecule in the inactivation and excretion of toxic substances [21, 22]. DPEP1 is a glycosylated homodimer present in lungs, liver, brain and highly expressed in the brush border of proximal tubular epithelial cells of the kidney [23–25].

DPEP1 has been shown to be a valuable target for preventing nephrotoxicity induced by platin derivatives [26–29]. Based on this fact, we hypothesized that DPEP1 could be involved in OxPt neurotoxicity, and this could be prevented by the use of DPEP1 inhibitors, as cilastatin [26]. However, very little is known about DPEP1 expression in DRG cells. In order to study DPEP1 protein, as a first stage, we generated a series of DPEP1 specific polyclonal antibodies, then, our goal was to describe the expression at cellular and subcellular levels of DPEP1 in rat DRG and possible changes in the inflammation elicited by OxPt in the short time period (six days) after OxPt treatment.

DRG is formed mainly by neurons of small, medium and large sizes, surrounded by glial cells, within a basket of capillary blood vessels and some Schwann cells that wrap the axons of neurons in roots [30]. To study molecular variations in this functional and morphological complex structure, the use of regular methods, such as western blots or PCR techniques, do not allow us to know what the specifically damaged cells are, or if all cells are affected. Instead, we decided to use confocal microscopy with well characterized specific antibodies. This study reports the expression DPEP1 in all types of neurons, glia, endothelial and Schwann cells in control rats and after a single dose of oxaliplatin and the inflammation response in DRG in the short term toxicity of OxPt.

Methods

DPEP1 antisera production and testing for specificity

DPEP1 peptide designing, plasmid construction and recombinant DPEP1 protein production and purification

In order to assess the homology of DPEP1 between human and rat at the protein level, Sequence Alignment command from sequence analysis tools from EMBL-EBI was performed (Figure S1 in Supplementary material). DPEP1 sequence was amplified from human kidney cDNA by PCR using Phusion polymerase (Thermo Scientific, Waltham, MA, USA) following the manufacturer's instructions. DPEP C-terminus coding region was amplified corresponding to a 419 pb Bam-HT/EcoR1I fragment (DPEP1-C; F2=CGGGATCCCGCTGGTG AAACAGACAGACAG) (Fig. 2A). After cloning into pRSET-c expression vector (Invitrogen, Carlsbad, CA, USA) sequence fidelity was tested by sequencing. The recombinant protein was expressed in Escherichia coli BL21(DE) cells by induction with 1 mM isopropyl-β-d-thiogalactopyranoside (IPTG) at 37 °C for 4 h. Purification of the recombinant protein was performed using HisTrap FF column (GE Healthcare, Little Chalfont, UK) following the manufacturer's instructions.

Production and purification of polyclonal antibodies against DPEP1

Antisera against human recombinant DPEP1-C were raised in male New Zealand rabbits in La Laguna University Animal Care Facility. Animal care and experimental procedures used for this work were approved by the Institutional Animal Care and Use Ethical Committee at the University of La Laguna. Preimmune serum was

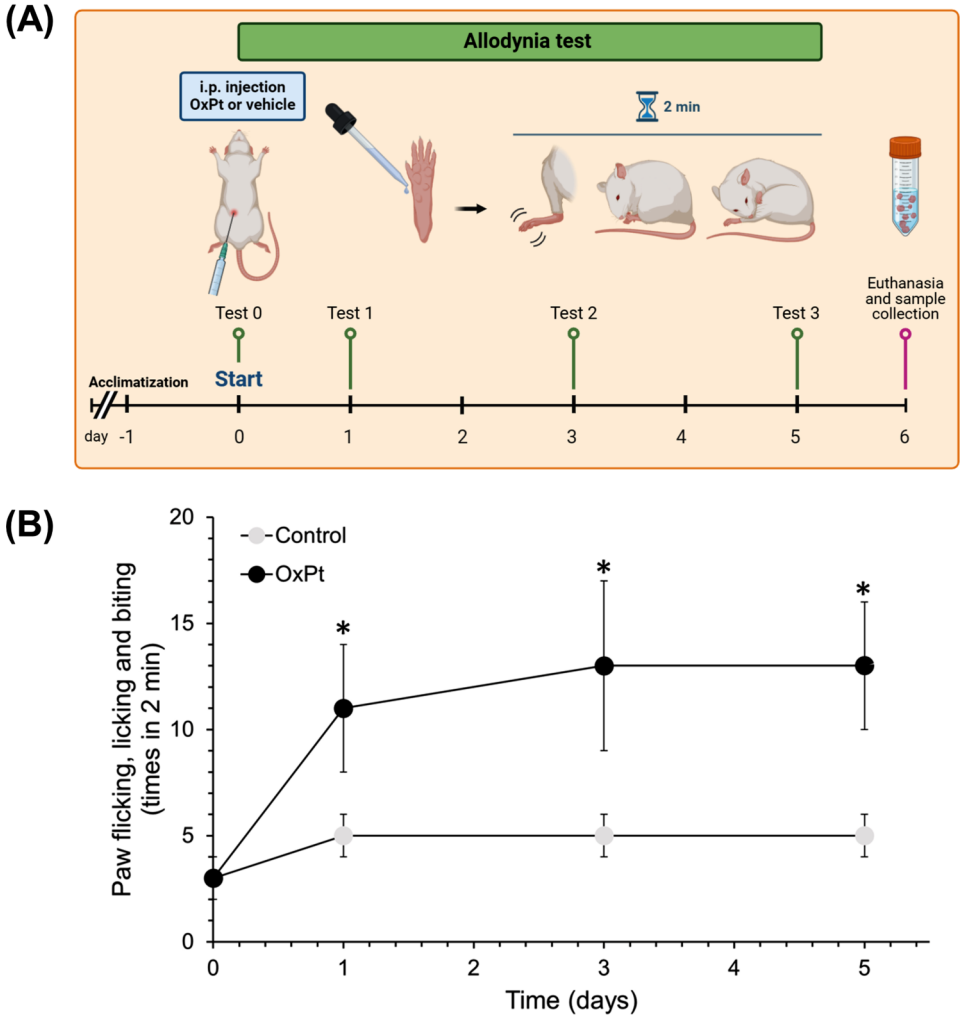

Fig. 1 (**A**) Diagram of the experimental timeline of the study. (**B**) Evaluation of cold hyperalgesia (allodynia) in controls and in OxPt rats. Acetone test was performed at 0, 1, 3 y 5 days. The data are expressed as the mean ± SEM, * indicates statistical significance $p < 0.05$. i.p., intraperitoneal, OxPt, oxaliplatin

collected and treated as described above for the DPEP1 serum, before injecting the immunogen. Purified recombinant protein (200 µg) emulsified with an equal volume (0.5 mL) of Freund's complete adjuvant was injected subcutaneously. Two additional injections were given with a ten-day interval, with 100 µg recombinant protein mixed with incomplete Freund's adjuvant in same proportions. Ten days after the final injection, blood was collected and clotting allowed for one hour at 37 °C and overnight at 4 °C. Antiserums were collected by centrifugation (7000× g, 5 min).

Purification of anti-DPEP1 antibodies was performed using HisTrap FF column (GE Healthcare, Little Chalfont, UK) linked to DPEP1-C recombinant protein. After passing the serum through the column, specific antibodies retained were eluted with 100 mM glycine pH 2.5 (AbDPEP1). Neutral pH was restored by adding 1/10 of total volume of 1 M Tris buffer pH 8. Antibodies were further purified using Protein G MagBeads (GenScript, Piscataway, NJ, USA) following manufacturer's instructions.

Antisera testing by western blot

Rat kidney pieces were homogenized by grinding in liquid nitrogen. Protein extract in Laemmli Sample Buffer were electrophoresed on a denaturing 12% polyacrylamide gel and transferred to Immobilon™-P membranes (Millipore, Bedford, MA, USA) by electroblotting. Membranes were blocked in PBS/5% BSA for 1 h. Protein detection was performed using DPEP1-C antibodies (1:2000; P. Martín-Vasallo/J. Ávila) and anti-rabbit Ig Horseradish peroxidase (GE Healthcare, Little Chalfont, UK) secondary antibody. Detection was performed using ECL plus (GE Healthcare, Little Chalfont, UK) reagents, according to the manufacturer's instructions, in a Chemi-Doc XRS (Bio–Rad Laboratories, Hercules, CA, USA).

Experimental design, animals and OxPt-induced neuropathic allodinya

For the pilot model, we used 18 male Wistar rats (10 treated with OxPt and 8 controls) weighing approximately 250 g (8 weeks old) at the beginning of the study, supplied by Instituto de Investigación Sanitaria Gregorio Marañón animal facility (Madrid, Spain). All animal handling was carried out according to the current legal regulations on the protection of animals used for experimental and other scientific purposes: RD 118/2021, of 23 February; Law 32/2007, of 7 November and order ECC/566/2015, of 20 March. Based on recent results showing sex dimorphism in rodents in inflammatory pain regulation and in immune cell signaling in neuropathic pain [17, 31], we decided to use males, as other models for chemotherapy induced PN did [15, 16, 18].

Rats were stabled in conventional cages in pairs, without food/water restriction, stable temperature, and humidity conditions (T=22±2ºC and HR=45–65%). OxPt was supplied by the Hospital Gregorio Marañón Pharmacy Service, at an initial concentration of 2 mg/mL dissolved in 5% glucose solution (Braun Medical S.A., Barcelona, Spain) and administered at a final concentration of 6 mg/kg, in a single dose injected peritoneal, at the beginning of the study that lasted 6 days. Figure 1, panel A shows a diagram of the experimental timeline.

The eight non-treated animals included in this study as control group were injected with the same vehicle, in the same conditions and volumes as the treated group.

Allodynia test of OxPt peripheral neurotoxicity

Cold allodynia (assessment of thermal sensation) was tested with the acetone test performed on days 0, 1, 3 and 5 by touching the plantar skin of both hind paws with a 200 µL droplet of acetone (PanReac, Barcelona, Spain) [32] from an insulin-type syringe (B.Braun Medical S.A., Madrid, Spain). The times of twitching and biting or licking the stimulated paw were counted for 2 min. The times were considered as the media of testing three times at a 1-hour interval.

Tissue collection

On day 6, euthanasia took place. Rats were anesthetized with sevorane (AbbVie Spain, Madrid, Spain) at 5% and maintenance during surgery at 2%. Animals were placed in the surgical field and the hair was opened with scissors along the spine in a distal direction and the spine was isolated by cutting on both sides, along the spine beyond the pelvic bone. For ethical purposes, we would like to assess that after spine bone removal from cervical region, animals were decapitated under anesthesia. The cervical vertebrae were removed and completely cleaned. The lumbar DRGs and the sciatic nerve were located and removed. These samples were introduced in 4% paraformaldehyde (PFA, Santa Cruz Biotechnology, Texas, USA) for 24 h at 4 °C for fixation and then were placed in 70% ethanol denatured ACS (denatured with 5% isopropanol and 5% methanol, VWR Chemicals BDH®, USA) until subsequent histological study.

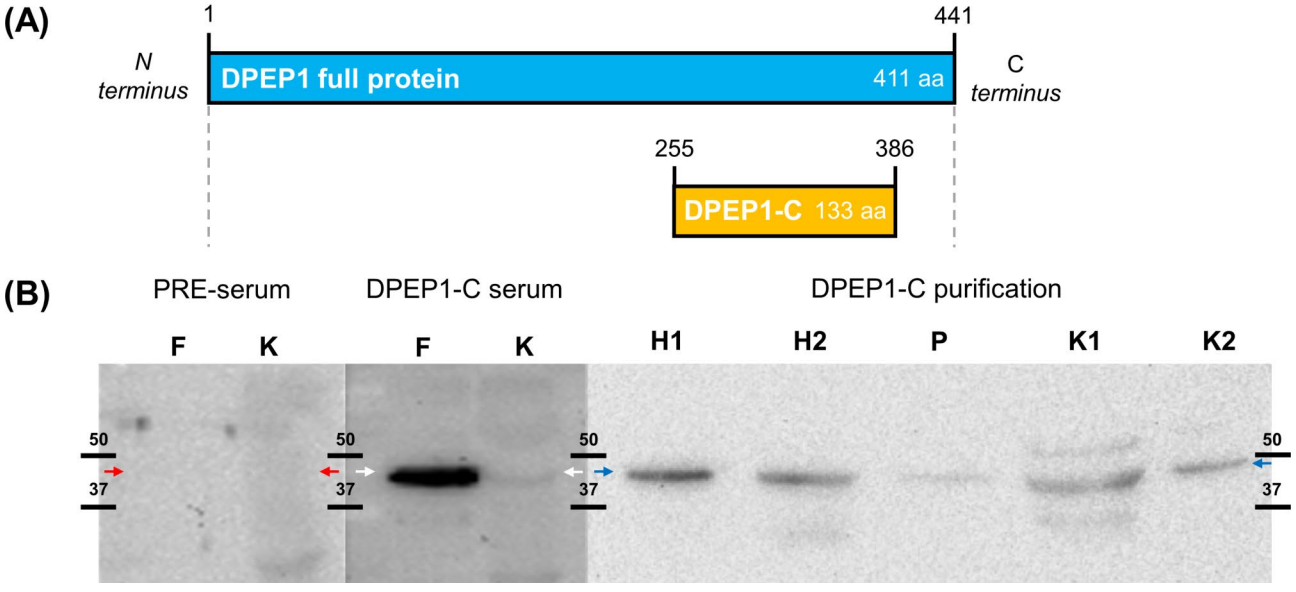

Fig. 2 Protein engineering for antisera generation and antibody testing. (**A**) scheme of DPEP1-C peptide produced as immunogen for antisera generation. (**B**) Left panel, western blot probed with pre-immune sera (PRE-serum); red arrows point to the absence of bands at DPEP1. Middle panel, western blot probed with DPEP1-C antiserum; white arrows point to a 47 kDa band corresponding to DPEP1 recombinant protein (full protein), column F, and the rat DPEP1 isoform in kidney lysates (column K). Right panel, western blot probed with anti-DPEP1-C after antibody purification; blue arrows point to bands corresponding to DPEP1 in different samples: HeLa cells lysates (H1, H2), rat pancreas lysates (P), rat kidney lysates (K) and dehydropeptidase 1 (DPEP1)

Immunohistochemistry

DRG tissues samples were embedded in paraffin and cut with a five-micron thick. Tissue sections were deparaffinized in xylene and rehydrated in a 100%, 96% and 70% alcohol bath, sequentially. Epitope retrieval was performed by heating samples in sodium citrate buffer (pH 6.0) at 120 °C for 10 min in an autoclave. Then non-specific sites were blocked with 5% bovine serum albumin or serum in Tris-buffered saline (TBS) for 1 h at room temperature.

Finally, for the immunofluorescence staining tissue sections were incubated with primary antibodies (DPEP1-C 1:100 P. Martín-Vasallo/J. Ávila); MAP2 (microtubule-associated protein 2) 1:500 [Cat #MAB378]; GFAP (glial fibrillary acidic protein) 1:100 [Cat #sc-33673]; CD31 (cluster of differentiation 31) 1:150 [Cat #sc-376764]; TNF-α (tumor necrosis factor alpha) 1:150 [Cat #sc-52B83]; IL-6 (interleukin-6) 1:200 [Cat #sc-28343]) over night at 4 °C, simultaneously with a mixture of two case of double immunostaining. Samples incubated without primary antibodies were used as negative control. Slides were incubated for 1 h at room temperature in dark with secondary antibodies raised in different species and conjugated to different fluorochromes (FITC conjugated against rabbit [Cat #F9887] and DyLight®650-conjugated against mouse [Cat # ab97018]). Slides were mounted with ProLong®Diamond Anti-fade Mountant with DAPI (Molecular Probes by Life technologies) to visualize cell nuclei.

Microscopy

Slides were analyzed and digital images were captured using Zeiss LSM980 Airyscan-2 (Zeiss, Oberkochen, Germany) and Leica SP8 (Leica Microsystems, Wetzlar, Germany) confocal microscopes. Raw images in Carl Zeiss Image Data File (CZI) or Leica Image Format (LIF) were exported as Joint Photographic Experts Group (JPEG) at 300ppi. Figures were assembled using Adobe Photoshop CC 2018 and exported at 300ppi.

Image quantitative analysis

Image analysis was carried out using ImageJ software (National Institutes of Health; Bethesda, MD) with the EzColocalization plugin [33]. Confocal images used for analysis were taken using the same parameters. Laser power and detector gain settings were optimized to cover fluorescence signals in a 16-bit depth range without saturation. Changes in fluorescence from baseline were measured as mean intensity of selected regions of interest. Complementary, "Cell Counter" plug-in was used to ensure that neurons or glia were counted only once.

Statistics

Statistical analysis was carried out using SPSS version 25 for Windows (IBM Corp., Armonk, NY, USA). Acetone test data are presented as mean ± standard error of the mean (SEM). Values were subjected to one way analysis of variance (ANOVA) followed by Newman-Keuls test. A probability value (p) < 0.05 was considered statistically significant.

For the analysis of immunohistochemistry data, dependence test (chi-square) was performed between the staining levels of each group of cells, and non-parametric Kruskall-Wallis test was used to analyze significant differences in the distribution of staining levels with respect to cell type [34]. $p < 0.05$ was considered statistically significant.

Results

Oxaliplatin treated rats developed cold allodynia

No mortality, diarrhoea nor sign of alopecia were observed in any group of animals throughout the duration of the study. The rats were weighed before the administration of chemotherapy to record the baseline and every day of the study. No significant increase nor reduction in body weight was evident in rats during the time of the study. All OxPt-treated rats showed increased sensitivity to cold as evaluated by the acute nocifensive response to acetone test on days 1, 3 and 5. Following acetone cold stimulation, an observer, unaware of the rat group conditions, evaluated the test by counting the number of times of the response as flicking, licking or biting the tested paw increased by a factor of two to four (Fig. 1, panel B). OxPt treated animals showed higher sensitivity to acetone drops by flicking, licking or bitting their paws. The number varied from 3 to 6 times/2 mins in controls to 8 to 18 in rats undergoing OxPt.

Anti-DPEP1 antibody specificity

Scheme of the region of DPEP1 recognized by generated serum is shown in Fig. 2A. In order to check the specificity of the antibodies against recombinant DPEP1-C terminus (DPEP1-C), serum was used to probe western blots with *E. coli* recombinant protein and rat kidney lysates. Additionally, pre-immune serum was also checked. Pre-immune serum recognized neither the recombinant protein nor any other protein in rat kidney lysates (Fig. 2B). DPEP1-C antisera recognized the recombinant full protein and one band in rat kidney lysates at 47 kDa molecular radius (Mr) (Fig. 2B). Used rat tissue samples is justified by the high homology (almost 74%) between human and rat sequences (Figure S1 in Supplementary material).

DPEP1 cellular and subcellular distribution in control rat DRG probed by DPEP1-C antisera

To check the performance of DPEP1-C antiserum in DRG, immunohistochemistry preparations were carried out. Fluorescence signal was found distributed all over neurons with heterogeneous dot pattern at medium to high level of fluorescence intensity in cytosol and showing brighter signal in nucleolus (Fig. 3). Fluorescence was also evident in axons of the root (yellow arrowheads of Fig. 3). The signal for DPEP1-C antiserum was homogeneous among neuron cells, independently of marked differences among cells for MAP2 fluorescence signal.

Immunofluorescence signal for DPEP1-C in cells surrounding the neurons was found at high and medium level as well as in capillary vessels and presumably Schwann cells of root at low and medium levels and with brighter staining intensity in nuclei of glia and blood vessels (white arrows of Fig. 3).

Immunofluorescence for MAP2 showed heterogeneous localization, with higher intensity in cytosol of some neurons and lower in others.

Negative controls for immunohistochemistry images are shown in Figure S2 of Supplementary material.

DPEP1 expression and inflammation state in OxPt-treated rat DRG

DPEP1-C immunolabeling in control panels exhibited low-medium fluorescence intensity inside nuclei and medium-high intensity in the cytosol of neurons. The expression pattern of DPEP1 in DRG changed in OxPt treated rats, as reveled by DPEP1-C immunofluorescence signal of higher intensity inside neuron nuclei (Fig. 4).

The inflammatory state of cells was assessed by checking TNF-α and IL-6 proteins expression. Low level of specific immunofluorescence signal for TNF-α was found in control panels. Medium to high intensity was displayed in few endothelial cells (white arrows of Fig. 4) or axon fibres, or cells surrounding fibres of the roots (red arrowheads, Fig. 4). In control samples, there was no signal for TNF-α inside neurons (yellow stars in upper panels of Fig. 4). DRGs from OxP-treated rats exhibited prominent higher intensity signal level for TNF-α in the cytosol of neurons and low intensity inside nuclei; in Fig. 4, panels below, yellow arrowheads point to areas of higher TNF-α fluorescence inside neuron cells). Some vacuoles or vacuole-like structures are observed in cytosol of neurons (lower panels in Fig. 4). Signal intensity for TNF-α was increased in endothelial cells of OxPt-treated rats compared those of the control group. Axons in the root and presumably surrounding Schwann cells showed increased TNF-α signal at medium level (Fig. 4, red arrowheads).

Low-medium intensity immunostaining was found for IL-6 in endothelial cells of control panels (Fig. 5, white arrows). There was no signal for IL-6 in neurons nor in glial cells (yellow stars, upper panels of Fig. 5). OxPt-treated rat DRG panels revealed lower intensity for IL-6 in endothelial cells and slightly higher intensity inside neurons and glia cells (arrowheads, lower panels in Fig. 5). DPEP1-C immunofluorescence signal levels were variable from low to high intensity and homogeneous in both panels.

Expression in satellite glial cells of DPEP1: DPEP1-C and GFAP immunostaining in control and OxPt-treated rat DRG

Immunostaining localization and fluorescence levels of DPEP1-C were consistent with abovementioned images in control rat DRG (Fig. 6 upper panels). Fluorescence for DPEP1-C was found in cytosol of virtually all cells at variable-high level (yellow arrowheads, Fig. 6), and in tubular structures where GFAP signal was negative (white arrowheads, Fig. 6) corresponding to axons constituting the root of the nerve.

DPEP1-C signal conveyed similar intensity levels in OxPt-treated rat DRG. High intensity level in nuclei of some glia cells and cytosol of few neurons in similar localization to that of controls, but at a slightly increased intensity level (lower panels of Fig. 6). DPEP1-C specific fluorescence in some neurons showed a mesh pattern in

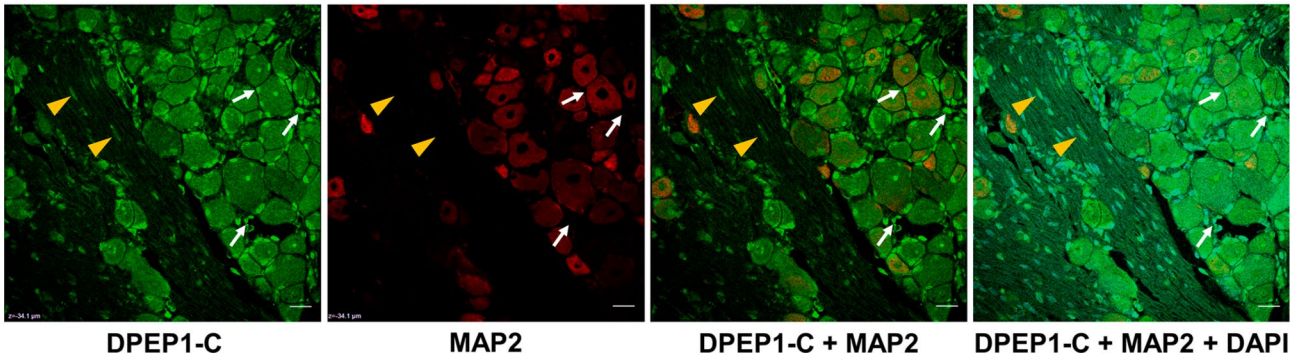

Fig. 3 Immunostaining of control rat DRG and root with DPEP1-C generated antisera. Green signal DPEP1-C, red signal MAP2 (neurons). Heterogeneous DPEP1-C immunofluorescence dot pattern in cytosol and higher staining intensity in nuclei of neurons, as well as glia cells (white arrows). Yellow arrowheads point to DPEP1-C fluorescence signal in axons and root cells. Leica SP8 confocal microscope. Bar = 40 µm

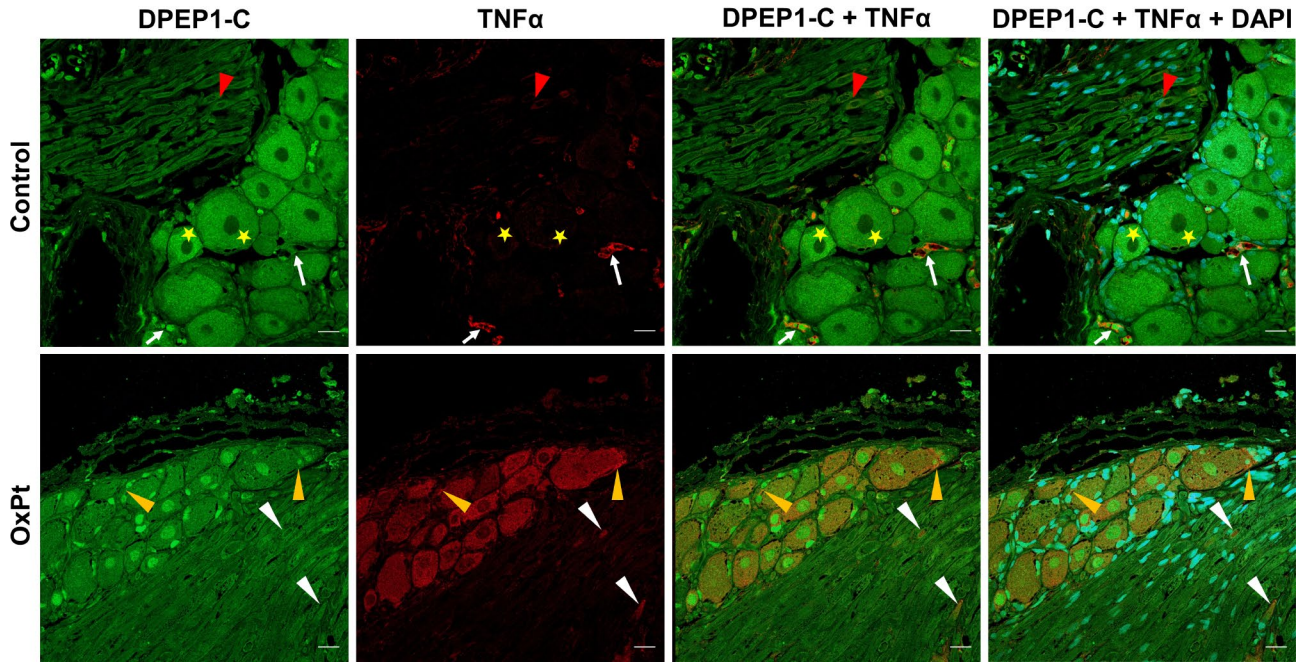

Fig. 4 Co-immunostaining for DPEP1 (green) and TNF-α (red) in control and OxPt-treated rat DRG. Control: low TNF-α fluorescence signal as spots in cytosol of neurons (yellow stars), axon fibres and surrounding cells (red arrowheads), few spots can be found in cells bordering neurons (white arrows). OxPt-treated DRG neurons show increased fluorescence signal for TNF-α (red), in cytosol, varying from low to high. Increased levels of TNF-α-specific fluorescence in glia cells (yellow arrowheads). Some vacuoles or vacuole-like structures in cells of OxPt treated rats. Zeiss LSM980 Airyscan-2 confocal microscope. Bar = 40 µm

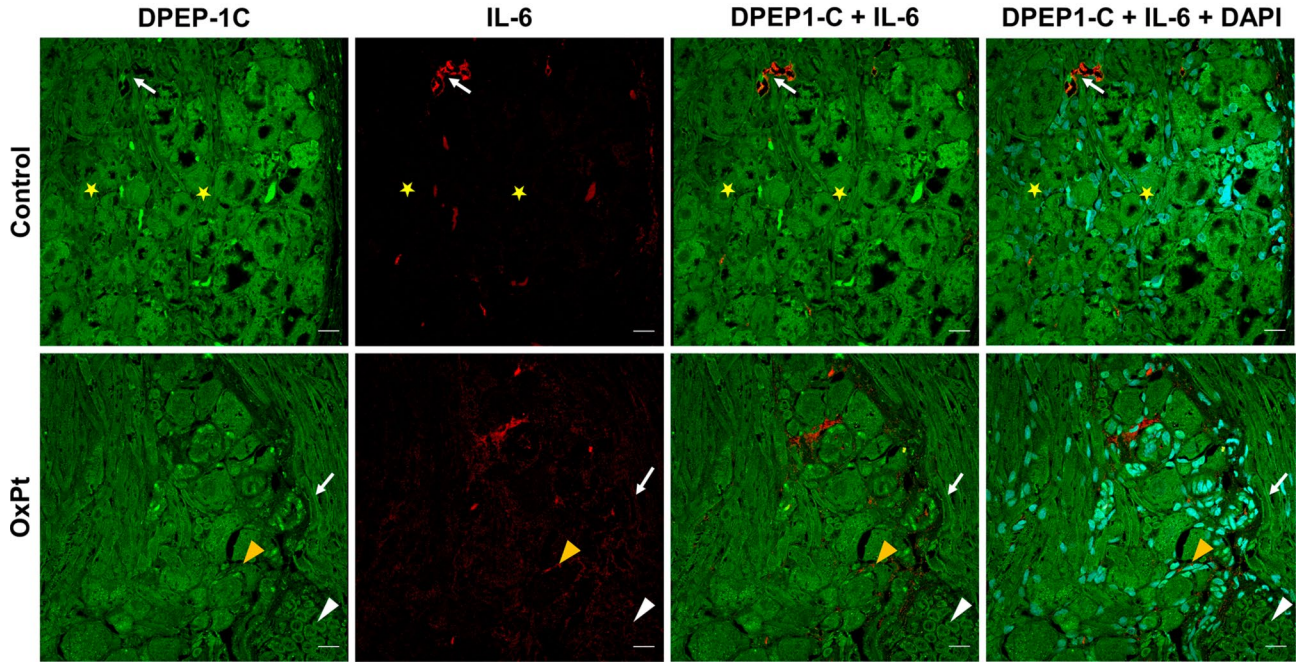

Fig. 5 Co-immunostaining for DPEP1 (green) and IL-6 (red) in control and OxPt-treated rat DRG. Control: IL-6 positive (red) in few endothelial cells of control panels (white arrows) and faint or no signal in neurons and in glia cells in (yellow stars). DRG from OxPt-treated rat: shows low intensity for IL-6 in the periphery of neurons and glia cells (yellow arrowheads) and in axons of root, either in longitudinal (white arrows) or transversal sections (white arrowheads). DPEP1-C and IL-6 fluorescence signals colocalize (DPEP1-C and IL-6 panels, due to difference in intensity signals this fact is barely shown in merges). Zeiss LSM980 Airyscan-2 confocal microscope. Bar = 40 µm

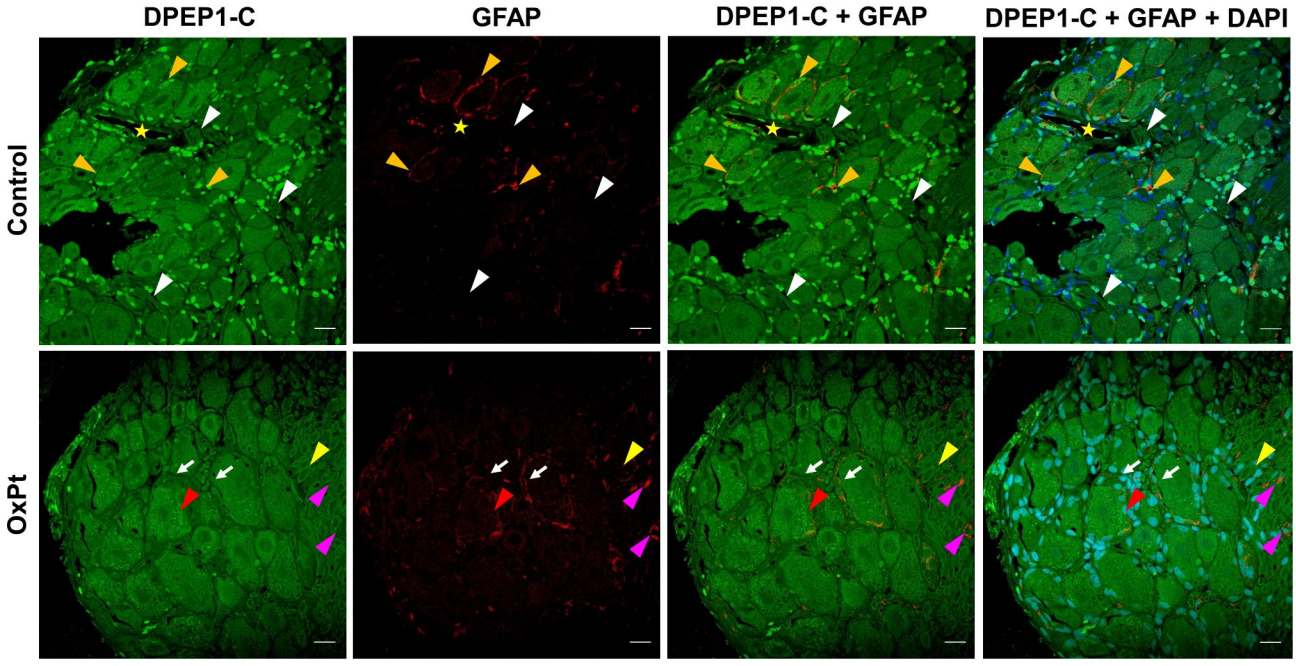

Fig. 6 Immunostaining for DPEP1-C and GFAP. Controls: yellow arrowheads point to GFAP signal (red), around neurons, apparently in cytosol of glia cell, colocalizing with DPEP1-C specific fluorescence (green) in cytosol and in the periphery of nuclei. White arrowheads point to DPEP1-C positive and GFAP negative tubular structures (axons); magenta arrowheads point to presumably activated Schwann cells. Yellow star is inside a blood vessel. OxPt treated rats: white arrows point to GFAP positive cells. Mesh pattern of DPEP1-C fluorescence in some neurons (red arrowheads). Yellow arrowheads point DPEP1-C cells in tubular structures (axons of root). Zeiss LSM980 Airyscan-2 confocal microscope. Bar = 40 µm

cytosol (red arrow in lower panels of Fig. 6), though in not all neurons, over a homogeneous background signal. GFAP positive immunolabeling was mainly present in small areas in cytosol of satellite glia cells (SGCs), at levels ranging from low to high intensity signal (white arrows in Fig. 6). GFAP+immunofluorescence was found in roots, at much higher intensity in samples from OxPt treated rats (magenta arrowheads in Fig. 6), marking presumably activated Schwann cells.

Blood vessel endothelial cells in control and OxPt-treated rat DRG

To show localization in the blood vessel structure and possible changes, DPEP1-C and CD31 immuno-costaining was performed. Control and OxPt rat DRG showed homogeneous immunofluorescence signals for CD31 antiserum. Nerve areas and root, with higher blood vessel density, showed higher intensity level of CD31 signal, as depicted in Fig. 7. Labeling for CD31 in DRG region varied from faint to bright, bordering neurons. Control panels showed higher intensity of DPEP1-C signal in endothelial cells nuclei (red arrowheads in upper panels of Fig. 7). In OxPt-treated rat DRG immunostaining for CD31 revealed distribution similar as that of control group, however, fluorescence in cells of the root was brighter than that of cells in roots of the control group; DPEP1-C was as described in previous images, with higher level inside nuclei than in control rat DRG samples.

Fig. 8 summarizes DPEP1 and TNF-α results at the cellular and subcellular differential expression.

Discussion

In this study we explored the cellular and subcellular localization of DPEP1 in DRG from normal rats and early (six days) changes elicited after OxPt chemotherapy treatment. Acetone test to allodynia confirmed peripheral neurotoxicity (Fig. 1) that was further supported morphologically by a striking increase of TNF-α expression as marker of acute inflammation of the DRG (Fig. 4).

First, we generated specific antisera against DPEP1. Antisera presented in this study were generated against human isoform, however, as shown in Figure S1, due to the high sequence homo either for immunohistochemistry or in western blot, they also recognize the rat isoform of DPEP1 at dilutions as high as 1:2000. At the time of the DPEP1 antiserum described in this study, there were no commercial antibodies against DPEP1. Some commercial antibodies were tested, such us anti-DPEP1 anti-body MBS2521928; BioSource (actually discontinued), but the results obtained were poor, showing less specificity in the recognition of the specific protein than DPEP1-C antiserum (data not shown). DPEP1-C antiserum presents a reliable performance in western blots as well as in

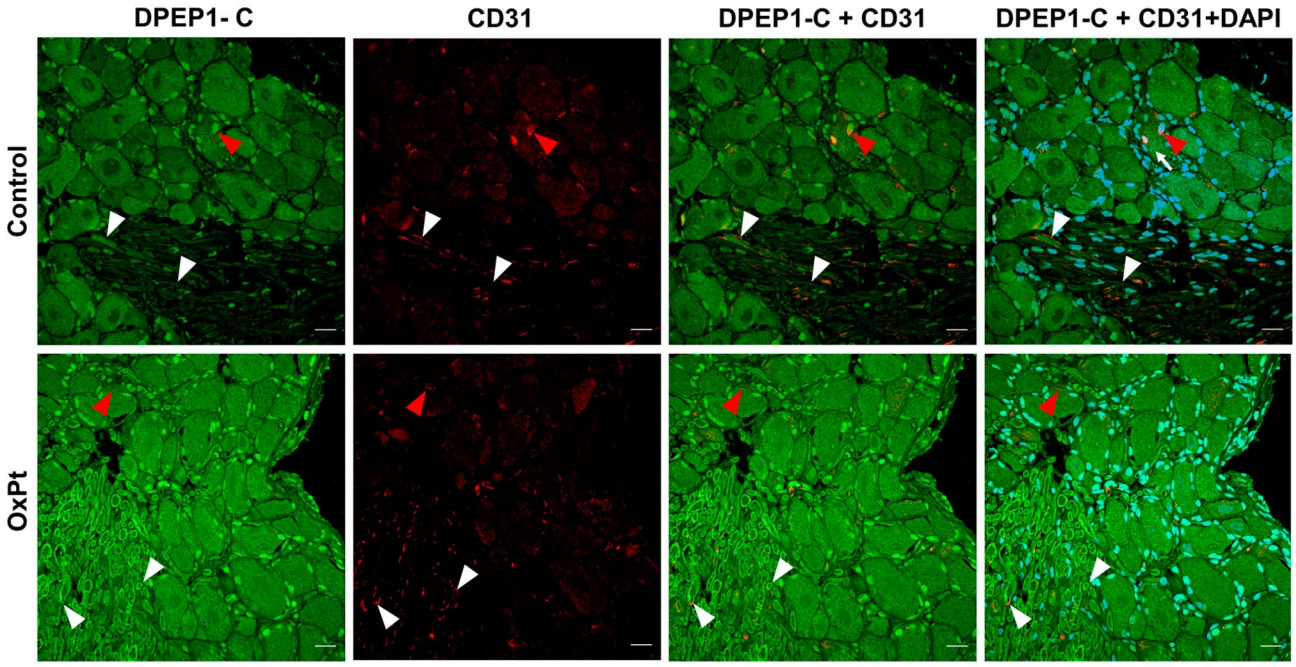

Fig. 7 Immunostaining for DPEP1-C and CD31 in control and OxPt-treated rat DRG. Red arrowheads point to CD31 + surrounding neurons and white arrowheads point to CD31 + fluorescence bordering axons in roots. Co-staining for DPEP1-C with CD31 pointed by white arrowheads in lower panels. Zeiss LSM980 Airyscan-2 confocal microscope. Bar = 40 µm

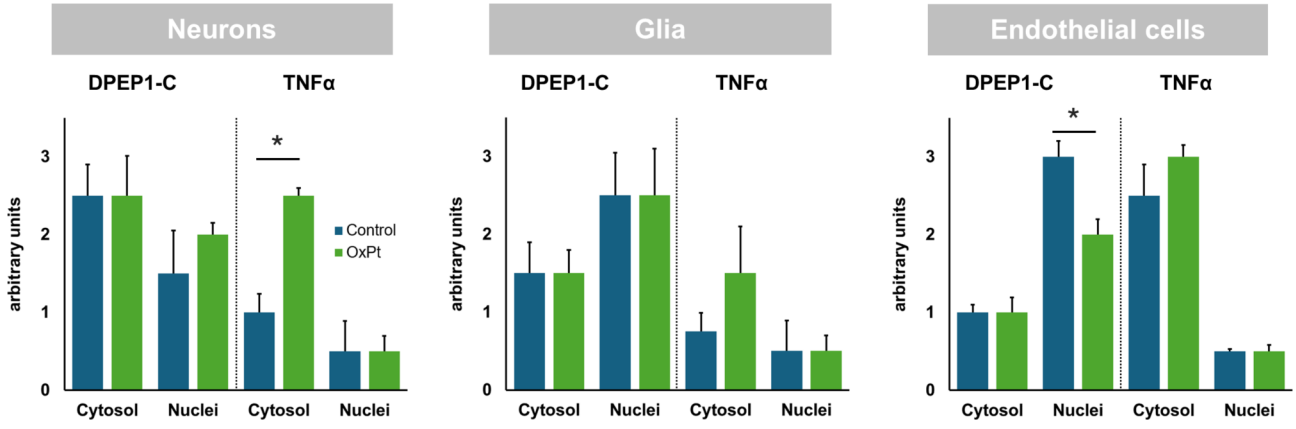

Fig. 8 Intensity of specific fluorescence signal for DPEP-1 C and TNF-α in DRG neurons, satellite glial cells (glia) and endothelial cell in control and OxPt-treated groups of rats. A significant increase in TNF-α was observed in neurons and a reduction of DPEP1 in endothelial cells following OxPt treatment when compared with the vehicle-treated group. The data are expressed as the mean ± SD, * indicates statistical significance $p < 0.05$

immunohistochemistry techniques, therefore, after evidencing a good quality and differential signal, either for cellular and subcellular localization (Figs. 2 and 3), we decided to use it in our experiments.

To further contrast our results, we use two different confocal microscopes, Leica SP8 and Zeiss LSM980 Airyscan-2, finding no differences in our results, however, given the better resolution of the Airyscan-2, most of the results published here were obtained with it.

To our knowledge, DPEP1 expression in DRG or peripheral nervous system (PNS) has not been described previously. There is only data about DPEP1 in brain capillaries and absence of enzymatic activity [25].

Previous studies revealed molecular changes in DRG after a single or two doses of OxPt, not only in neurons but also in glial cells [35]. However, the effect of this xenobiotic in the PNS is still controversial. Warwick et al. [36] demonstrated increased expression of GFAP in SGCs over twofold compared to control after two doses of OxPt. In the spinal cord, OxPt effects were similar according to Ahn et al. [37] and Yoon et al. [38] who showed that a single intraperitoneal injection of OxPt

(6 mg/kg) can induce mechanical and cold allodynia, accompanied to raised GFAP expression. This contrasts with more recent studies of Huang et al. [39] who demonstrated a reduction of GFAP expression seven days after a single dose of OxPt (6 mg/kg). In our study, there were no significant changes in GFAP immunofluorescence signal six days after a single dose of OxPt (6 mg/kg), therefore the role of GFAP in OxPt-induced PN remains uncertain.

GFAP molecular expression has been related to activation of glial cell types as astrocytes and SGCs after neuronal injury or inflammatory processes [35, 40–42]. Different studies have demonstrated acute glial activation after chemotherapy treatment with paclitaxel or OxPt [43, 44], coexisting with an elevation of proinflammatory cytokines from early stages, as TNF-α and later, as IL-6 [44, 45] in DRG structure. Xu et al. [45] found increased levels of these cytokines three days after a single dose of OxPt and an evident elevation of the expression of membrane receptors. Furthermore, an activation of Schwann cells with concomitant release of cytokines after PNS damage has been reported [46, 47]. Schwann cells, along with macrophages, constitute the main source of TNF-α after sciatic nerve injury [47]. Our results show significant increase of TNF-α in OxPt DRG in comparison with control DRG, not only in neurons but also in glial cells (Fig. 4). However, as shown in Fig. 4, TNF-α immunofluorescence signal is not homogeneous in all neurons, some neurons and glial cells expression levels range from high intensity to low, and some very light or nothing. This distribution gives an idea of "focality" of the damage, similar to what has been reported for kidney tubular nephrotoxicity induced by cisplatin [28]. Our experiments show increased signal levels for IL-6 in DRG from OxPt-treated rats at a slightly but evident proportion, probably due to the short-time effect of OxPt and considering IL-6 a long-period of inflammation marker. According to our results and those of consulted bibliography, most cells within the environment of DRG neurons have a relevant role in the pro-inflammatory state of OxPt-induced PN. The focal distribution of inflammation could be an indicative of different DRG neuron types affected by OxPt. Further studies exploring with specific markers for large-diameter myelinated Aβ-fibres, small-diameter myelinated (Aδ), and unmyelinated (C) need to be performed in order to determine the different sensitivities to inflammation of neurons [48].

DPEP1 has a heterogeneous distribution in DRG, with different location and expression depending on cell types, partially summarized in Fig. 8. Three types of neurons and six subtypes have been described in rat DRG based on its location, amount and structure of organelles and neurofilaments in the cytosol [30, 49]. The heterogeneous DPEP1 expression levels in neurons indicates functional differences among cells that also varies in OxPt chemotherapy; here we showed that DPEP1 is predominant in neuron cytosol in control samples, showing "granular" distribution (Fig. 6), and how high levels of DPEP1 immunofluorescence signal is found at in nuclei in DRG samples from OxPt-treated rats (Fig. 4). DPEP1 expression in nuclei suggests a moonlighting role of this protein, though further studies are needed to define its function.

Blood vessels in DRG and in peripheral nerves have a permeability that allows OxPt-chemotherapy entrance to PNS and accumulation in sensory neurons [50]. For this reason, it is remarkable the evident colocalization of DPEP1 and CD31 in endothelial cells, predominantly inside nuclei (Fig. 7). Choudhury et al. [51] showed DPEP1 as a physical adhesion receptor for neutrophils in mice lung and liver capillaries. This function was independent to its catalytic activity and contribute to inflammatory processes. Otherwise, the role of DPEP1 in immune response in DRG injury is still unknown.

The fact of finding DPEP1 expression in DRG neurons opens the prospect of this protein to be a target for peripheral neuropathy prevention, different from treatment of stablished pain, allodynia or neuropathy [12, 52]. Future research with DPEP1 inhibitors, such as cilastatin [29], will give us more information about possible peripheral neuroprotection by blocking DPEP1 and preventing totally or partially from the process of inflammation and cellular injury as adjuvant therapy to those that attenuate neuropathic pain [53, 54]. Complementarily, further studies on the DPEP1 role in DRG blood vessels and glia cells need to be addressed to understand the participation of these cells in PN.

Conclusions

This study reports the cellular and subcellular localization of DPEP1 in DRG in control rats and after short-term treatment of OxPt using specific polyclonal antibodies. DPEP1 is expressed in neurons, glia and endothelial cells of DRG. OxPt caused allodynia in rats and induced a high grade of inflammation within this short period with concurrent variable focal increase of TNF-α expression. In our model, OxPt induced GFAP expression in some cells of roots compatible with Schwann cells and does not affect MAP2 expression in neurons, nor GFAP in SGCs. The finding of DPEP1 in DRG opens the possibility of using this protein as target to avoid or minimize PN elicited by OxPt-based chemotherapy.

Supplementary Information

The online version contains supplementary material available at https://doi.org/10.1186/s12868-024-00891-y.

Supplementary Material 1

Acknowledgements
We thank Prof. Felipe Rosa, Department of Mathematics, Statistics and Operational Research, University of La Laguna, for statistical analysis and advice.

Author contributions
The conceptualization of this study was made by K.A-T., M.M., A.L. and P.M-V.; All experiments and data collection were carried out by K.A-T., R.G-F., M.A.G-N., R.M-R., R.G., M.R.A., F.M., J.A. and A.L..; Statistical analysis and interpretation of the data were performed by M.M., L.D-F., J.A., A.L. and P.M-V.; first draft was writing by K.A-T., R.G-F., M.A.G-N., R.M-R., M.M., R.G., L.D-F., M.R.A., F.M., J.A., A.L. ad P.M-V.; manuscript editing by K.A-T., R.M-R., A.L. and P.M-V.; This study was supervised by R.G-F., R.M-R., M.M., J.A. and A.L. All authors reviewed and approved the submitted manuscript.

Funding
This research was funded by grants numbers OA21/110 from Fundación MAPFRE-Guanarteme and PIFIISC22/34 from Fundación Canaria Instituto de Investigación Sanitaria de Canarias (FIISC) to MM, FM was supported by the Spanish Ministry of Science and Innovation (MCIN/AEI/https://doi.org/10.13039/501100011033) through the grant PID2021-123716OB-I100, cofinanced by the EU-ERDF "A way of making Europe"; Spanish Ministry of Economy and Competitiveness and Instituto de Salud Carlos III-Fondo de Investigación en Salud (grant numbers:, PI20/01577 and ICI21/00111 cofinanced by Fondo Europeo de Desarrollo Regional (FEDER) Funds from the European Commission, "A way of making Europe"), ISCIII-RICORS2040 (Kidney Disease, grant number RD21/0005/0029), Comunidad de Madrid (grant number 2022/BMD-7223 (CIFRA_COR-CM) to A.L.; and Gobierno de Canarias (cofounded by FEDER), grant number ProID2020010073 to J.A.

Data availability
No datasets were generated or analysed during the current study.

Declarations

Ethics approval and consent to participate
The study was conducted according to the guidelines of the Declaration of Helsinki and approved by the Institutional Review Board: The study was approved by the Institutional Board for Animal Experiments of the Gregorio Marañón Hospital Registration code 07-2008) and animals were handled at all times according to legal regulations stipulated by RD 118/2021, of 23 February.

Consent for publication
Not applicable.

Competing interests
The authors declare no competing interests.

Author details
[1]Laboratorio de Biología del Desarrollo, UD de Bioquímica y Biología Molecular, Universidad de La Laguna, San Cristóbal de La Laguna, Spain
[2]Unidad de Investigación, Hospital Universitario Nuestra Señora de la Candelaria, Instituto de Investigación Sanitaria de Canarias (IISC), Santa Cruz de Tenerife, Spain
[3]Departamento de Farmacia Hospitalaria, Hospital Universitario Nuestra Señora de la Candelaria, Santa Cruz de Tenerife, Spain
[4]Laboratorio de Fisiopatología Renal, Departamento de Nefrología, Instituto de Investigación Sanitaria Gregorio Marañón, Hospital General Universitario Gregorio Marañón, Madrid, Spain
[5]Departamento de Oncología Médica, Hospital Universitario Nuestra Señora de la Candelaria, Santa Cruz de Tenerife, Spain
[6]Departamento de Ciencias Médicas Básicas, Facultad de Ciencias de la Salud, Universidad de La Laguna, San Cristóbal de La Laguna, Spain
[7]Servicio de Estabulario y Animalario del Servicio General de Apoyo a la Investigación (SEGAI), Universidad de La Laguna, San Cristóbal de La Laguna, Spain
[8]Instituto de Tecnologías Biomédicas, Universidad de La Laguna, San Cristóbal de La Laguna, Spain
[9]Facultad de Ciencias de la Salud, Universidad Fernando Pessoa Canarias, Las Palmas de Gran Canaria, Spain
[10]Departamento de Fisiología, Facultad de Medicina, Universidad Complutense de Madrid, Madrid, Spain

Received: 22 April 2024 / Accepted: 5 September 2024
Published online: 15 September 2024

References

1. Pasetto LM, D'Andrea MR, Brandes AA, Rossi E, Monfardini S. The development of platinum compounds and their possible combination. Crit Reviews Oncology/Hematology. 2006;60(1):59–75.
2. Averin A, Silvia A, Lamerato L, Richert-Boe K, Kaur M, Sundaresan D, et al. Risk of chemotherapy-induced febrile neutropenia in patients with metastatic cancer not receiving granulocyte colony-stimulating factor prophylaxis in US clinical practice. Support Care Cancer. 2021;29(4):2179–86.
3. Morales M, Ávila J, González-Fernández R, Boronat L, Soriano M, Martín-Vasallo P. Differential transcriptome profile of peripheral white cells to identify biomarkers involved in oxaliplatin induced neuropathy. J Pers Med. 2014;4(2):282–96.
4. Ewertz M, Qvortrup C, Eckhoff L. Chemotherapy-induced peripheral neuropathy in patients treated with taxanes and platinum derivatives. Acta Oncol. 2015;54(5):587–91.
5. Kang L, Tian Y, Xu S, Chen H. Oxaliplatin-induced peripheral neuropathy: clinical features, mechanisms, prevention and treatment. J Neurol. 2021;268(9):3269–82.
6. Zamami Y, Niimura T, Kawashiri T, Goda M, Naito Y, Fukushima K, et al. Identification of prophylactic drugs for oxaliplatin-induced peripheral neuropathy using big data. Biomed Pharmacother. 2022;148:112744.
7. Argyriou A. Updates on Oxaliplatin-Induced Peripheral neurotoxicity (OXAIPN). Toxics. 2015;3(2):187–97.
8. Staff NP, Cavaletti G, Islam B, Lustberg M, Psimaras D, Tamburin S. Platinum-induced peripheral neurotoxicity: from pathogenesis to treatment. J Peripher Nerv Syst. 2023;24(S2).
9. Johnson C, Pankratz VS, Velazquez AI, Aakre JA, Loprinzi CL, Staff NP, et al. Candidate pathway-based genetic association study of platinum and platinum–taxane related toxicity in a cohort of primary lung cancer patients. J Neurol Sci. 2015;349(1–2):124–8.
10. Tiwari V, Guan Y, Raja SN. Modulating the delicate glial–neuronal interactions in neuropathic pain: promises and potential caveats. Neurosci Biobehav Rev. 2014;45:19–27.
11. Morales M, Staff NP. Treatment of established chemotherapy-induced peripheral neuropathy: basic science and animal models. Diagnosis, management and emerging strategies for Chemotherapy-Induced Neuropathy. Volume 1. Cham: Springer; 2021. p. 137–56.
12. Akhilesh UA, Mehta A, Tiwari V. Combination chemotherapy in rodents: a model for chemotherapy-induced neuropathic pain and pharmacological screening. Metab Brain Dis. 2023. https://doi.org/10.1007/s11011-023-01315-2
13. Miltenburg NC, Boogerd W. Chemotherapy-induced neuropathy: a comprehensive survey. Cancer Treat Rev. 2014;40(7):872–82.
14. Sałat K. Chemotherapy-induced peripheral neuropathy—part 2: focus on the prevention of oxaliplatin-induced neurotoxicity. Pharmacol Rep. 2020;72(3):508–27.
15. Gadepalli A, Ummadisetty O, Akhilesh CD, Anmol TV. Loperamide, a peripheral Mu-Opioid receptor agonist, attenuates chemotherapy-induced neuropathic pain in rats. Int Immunopharmacol. 2023;124:110944.
16. Gadepalli A, Ummadisetty O, Akhilesh, Chouhan D, Yadav KE, Tiwari V. Peripheral mu-opioid receptor activation by dermorphin [D-Arg2, Lys4] (1–4) amide alleviates behavioral and neurobiological aberrations in rat model of chemotherapy-induced neuropathic pain. Neurother. 2024;21(1):e00302.
17. Akhilesh UA, Gadepalli A, Tiwari V, Allani M, Chouhan D, et al. Unlocking the potential of TRPV1 based siRNA therapeutics for the treatment of chemotherapy-induced neuropathic pain. Life Sci. 2022;288:120187.
18. Akhilesh CD, Ummadisetty O, Verma N, Tiwari V. Bergenin ameliorates chemotherapy-induced neuropathic pain in rats by modulating TRPA1/TRPV1/NR2B signalling. Int Immunopharmacol. 2023;125:111100.
19. Wei G, Gu Z, Gu J, Yu J, Huang X, Qin F, et al. Platinum accumulation in oxaliplatin-induced peripheral neuropathy. J Peripher Nerv Syst. 2021;26(1):35–42.
20. Illias AM, Yu KJ, Hwang SH, Solis J, Zhang H, Velasquez JF, et al. Dorsal root ganglion toll-like receptor 4 signaling contributes to oxaliplatin-induced peripheral neuropathy. Pain. 2022;163(5):923–35.

21. Lecomte T, Landi B, Beaune P, Laurent-Puig P, Loriot MA. Glutathione S-Transferase P1 polymorphism (Ile105Val) predicts cumulative neuropathy in patients receiving oxaliplatin-based chemotherapy. Clin Cancer Res. 2006;12(10):3050–6.
22. Marmiroli P, Riva B, Pozzi E, Ballarini E, Lim D, Chiorazzi A, et al. Susceptibility of different mouse strains to oxaliplatin peripheral neurotoxicity: phenotypic and genotypic insights. PLoS ONE. 2017;12(10):e0186250.
23. Hirota T, Nishikawa Y, Tanaka M, Fukuda K, Igarashi T, Kitagawa H. Localization of dehydropeptidase-I, an enzyme processing glutathione, in the rat kidney. J Biochem. 1987;102(3):547–50.
24. Adachi H, Kubota I, Okamura N, Iwata H, Tsujimoto M, Nakazato H, et al. Purification and characterization of human microsomal dipeptidase. J Biochem. 1989;105(6):957–61.
25. Inamura T, Pardridge WM, Black KL. Differential tissue expression of immunoreactive dehydropeptidase 1,a peptidyl leukotriene metabolizing enzyme. Prostaglandins Leukot Essent Fatty Acids. 1994;50:85–92.
26. Humanes B, Camaño S, Lara JM, Sabbisetti V, González-Nicolás MÁ, Bonventre JV, et al. Cisplatin-induced renal inflammation is ameliorated by cilastatin nephroprotection. Nephrol Dial Transplant. 2017;32(10):1645–55.
27. Camano S, Lazaro A, Moreno-Gordaliza E, Torres AM, De Lucas C, Humanes B, et al. Cilastatin attenuates cisplatin-induced proximal tubular cell damage. J Pharmacol Exp Ther. 2010;334(2):419–29.
28. González-Fernández R, González-Nicolás MÁ, Morales M, Ávila J, Lázaro A, Martín-Vasallo P. FKBP51, AmotL2 and IQGAP1 involvement in cilastatin prevention of cisplatin-induced tubular nephrotoxicity in rats. Cells. 2022;11(9):1585.
29. Humanes B, Lazaro A, Camano S, Moreno-Gordaliza E, Lazaro JA, Blanco-Codesido M, et al. Cilastatin protects against cisplatin-induced nephrotoxicity without compromising its anticancer efficiency in rats. Kidney Int. 2012;82(6):652–63.
30. Haberberger RV, Kuramatilake J, Barry CM, Matusica D. Ultrastructure of dorsal root ganglia. Cell Tissue Res. 2023;393(1):17–36.
31. Luo X, Gu Y, Tao X, Serhan CN, Ji RR. Resolvin D5 inhibits neuropathic and inflammatory pain in male but not female mice: distinct actions of D-Series resolvins in chemotherapy-induced peripheral neuropathy. Front Pharmacol. 2019;10:745.
32. Mizuno K, Kono T, Suzuki Y, Miyagi C, Omiya Y, Miyano K, et al. Goshajinkigan, a traditional Japanese medicine, prevents oxaliplatin-induced acute peripheral neuropathy by suppressing functional alteration of TRP channels in rat. J Pharmacol Sci. 2014;125(1):91–8.
33. Stauffer W, Sheng H, Lim HN. EzColocalization: an ImageJ plugin for visualizing and measuring colocalization in cells and organisms. Sci Rep. 2018;8(1):15764.
34. Armitage P, Matthews JNS, Geoffrey B. Statistical methods in medical research. 4th ed. Wiley-Blackwell; 2001.
35. Lee JH, Kim W. The role of satellite glial cells, astrocytes, and microglia in oxaliplatin-induced neuropathic pain. Biomedicines. 2020;8(9):324.
36. Warwick Ra, Hanani M. The contribution of satellite glial cells to chemotherapy-induced neuropathic pain. Eur J Pain. 2013;17(4):571–80.
37. Ahn BS, Kim SK, Kim HN, Lee JH, Lee JH, Hwang DS, et al. Gyejigachulbu-Tang relieves oxaliplatin-induced neuropathic cold and mechanical hypersensitivity in rats via the suppression of spinal glial activation. Evid Based Complement Altern Med. 2014;2014:1–7.
38. Yoon SY, Robinson CR, Zhang H, Dougherty PM. Spinal astrocyte gap junctions contribute to oxaliplatin-induced mechanical hypersensitivity. J Pain, 2013;14(2):205–14.
39. Huang W, Huang J, Jiang Y, Huang X, Xing W, He Y, et al. Oxaliplatin regulates chemotherapy induced peripheral neuropathic pain in the dorsal horn and dorsal root ganglion via the Calcineurin/NFAT pathway. ACAMC. 2018;18(8):1197 – 207.
40. Jasmin L, Vit JP, Bhargava A, Ohara PT. Can satellite glial cells be therapeutic targets for pain control? Neuron Glia Biol. 2010;6(1):63–71.
41. Takeda M, Tanimoto T, Kadoi J, Nasu M, Takahashi M, Kitagawa J, et al. Enhanced excitability of nociceptive trigeminal ganglion neurons by satellite glial cytokine following peripheral inflammation. Pain. 2007;129(1):155–66.
42. Elson K, Speck P, Simmons A. Herpes simplex virus infection of murine sensory ganglia induces proliferation of neuronal satellite cells. J Gen Virol. 2003;84(5):1079–84.
43. Di Cesare Mannelli L, Pacini A, Bonaccini L, Zanardelli M, Mello T, Ghelardini C. Morphologic features and glial activation in rat oxaliplatin-fependent neuropathic pain. J Pain. 2013;14(12):1585–600.
44. Lees JG, Makker PGS, Tonkin RS, Abdulla M, Park SB, Goldstein D, et al. Immune-mediated processes implicated in chemotherapy-induced peripheral neuropathy. Eur J Cancer. 2017;73:22–9.
45. Xu D, Zhao H, Gao H, Zhao H, Liu D, Li J. Participation of pro-inflammatory cytokines in neuropathic pain evoked by chemotherapeutic oxaliplatin via central GABAergic pathway. Mol Pain 2018;14:174480691878353.
46. Bolin LM, Verity AN, Silver JE, Shooter EM, Abrams JS. Interleukin-6 production by Schwann Cells and induction in sciatic nerve Injury. J Neurochem. 2002;64(2):850–8.
47. Wei Z, Fei Y, Su W, Chen G. Emerging role of Schwann Cells in neuropathic pain: receptors, glial mediators and myelination. Front Cell Neurosci. 2019;13:116.
48. Smith ESJ, Lewin GR. Nociceptors: a phylogenetic view. J Comp Physiol. 2009;195(12):1089–106.
49. Rambourg A, Clermont Y, Beaudet A. Ultrastructural features of six types of neurons in rat dorsal root ganglia. J Neurocytol. 1983;12(1):47–66.
50. Jimenez-Andrade JM, Herrera MB, Ghilardi JR, Vardanyan M, Melemedjian OK, Mantyh PW. Vascularization of the dorsal root ganglia and peripheral nerve of the mouse: implications for chemical-induced peripheral sensory neuropathies. Mol Pain. 2008;4:1744-8069-4-10.
51. Choudhury SR, Babes L, Rahn JJ, Ahn BY, Goring KAR, King JC, et al. Dipeptidase-1 is an adhesion receptor for neutrophil recruitment in lungs and liver. Cell. 2019;178(5):1205–e122117.
52. Xu Z, Lee MC, Sheehan K, Fujii K, Rabl K, Rader G, et al. Chemotherapy for pain: reversing inflammatory and neuropathic pain with the anticancer agent mithramycin A. Pain. 2024;165(1):54–74.
53. Kono T, Suzuki Y, Mizuno K, Miyagi C, Omiya Y, Sekine H, et al. Preventive effect of oral goshajinkigan on chronic oxaliplatin-induced hypoesthesia in rats. Sci Rep. 2015;5(1):16078.
54. Gris G, Portillo-Salido E, Aubel B, Darbaky Y, Deseure K, Vela JM, et al. The selective sigma-1 receptor antagonist E-52862 attenuates neuropathic pain of different aetiology in rats. Sci Rep. 2016;6(1):24591.

Publisher's note

Springer Nature remains neutral with regard to jurisdictional claims in published maps and institutional affiliations.